The EMBO Journal (2010) 29, 2230–2241 | © 2010 European Molecular Biology Organization | All Rights Reserved 0261-4189/10
www.embojournal.org

THE EMBO JOURNAL

SNMIB/Apollo protects leading-strand telomeres against NHEJ-mediated repair

Yung C Lam[1], Shamima Akhter[1], Peili Gu[1], Jing Ye[2], Anaïs Poulet[2], Marie-Josèphe Giraud-Panis[2], Susan M Bailey[3], Eric Gilson[2,4], Randy J Legerski[1] and Sandy Chang[1,5,6,*]

[1]Department of Genetics Unit 1010, The U.T.M.D. Anderson Cancer Center, Houston, TX, USA, [2]Laboratory of Biology and Pathology of Genomes of University of Nice Sophia-Antipolis, CNRS UMR6267/ INSERM U998, Faculty of Medicine, Nice, France, [3]Department of Environmental and Radiological Health Sciences, Colorado State University, Fort Collins, CO, USA, [4]Department of Medical Genetics, CHU of Nice, France and [5]Department of Hematopathology, The U.T.M.D. Anderson Cancer Center, Houston, TX, USA

Progressive telomere attrition or deficiency of the protective shelterin complex elicits a DNA damage response as a result of a cell's inability to distinguish dysfunctional telomeric ends from DNA double-strand breaks. SNMIB/Apollo is a shelterin-associated protein and a member of the SMN1/ PSO2 nuclease family that localizes to telomeres through its interaction with TRF2. Here, we generated *SNMIB/Apollo* knockout mouse embryo fibroblasts (MEFs) to probe the function of SNMIB/Apollo at mammalian telomeres. *SNMIB/ Apollo* null MEFs exhibit an increased incidence of G2 chromatid-type fusions involving telomeres created by leading-strand DNA synthesis, reflective of a failure to protect these telomeres after DNA replication. Mutations within SNMIB/Apollo's conserved nuclease domain failed to suppress this phenotype, suggesting that its nuclease activity is required to protect leading-strand telomeres. *SNMIB/ Apollo*$^{-/-}$*ATM*$^{-/-}$ MEFs display robust telomere fusions when *Trf2* is depleted, indicating that ATM is dispensable for repair of uncapped telomeres in this setting. Our data implicate the 5′–3′ exonuclease function of SNM1B/Apollo in the generation of 3′ single-stranded overhangs at newly replicated leading-strand telomeres to protect them from engaging the non-homologous end-joining pathway.

The EMBO Journal (2010) **29,** 2230–2241. doi:10.1038/ emboj.2010.58; Published online 15 June 2010
Subject Categories: genome stability & dynamics
Keywords: chromosomes; DNA damage; telomeres

Introduction

Mammalian telomeres consist of TTAGGG repetitive sequences that terminate in a 3′ single-stranded (ss) G-rich overhang. Telomeres are bound and stabilized by a number of telomere-specific-binding proteins that form a core complex termed shelterin that protects telomeres from inappropriately activating the DNA damage response (DDR) (Palm and de Lange, 2008). Three sequence-specific DNA-binding proteins are recruited to chromosomal ends: the duplex telomere-binding proteins TRF1 and TRF2/RAP1, and the ss TTAGGG repeat-binding protein POT1. These proteins are interconnected by the adapter proteins TIN2 and TPP1. Telomeres rendered dysfunctional by the removal of TRF2/RAP1 activate ATM and are repaired by the non-homologous end-joining (NHEJ) pathway, whereas removal of the POT1–TPP1 complex activates NHEJ-mediated repair that requires ATR (Wu *et al*, 2006; Denchi and de Lange, 2007; Guo *et al*, 2007; Deng *et al*, 2009).

Emerging evidence suggests that the core shelterin complex is insufficient for complete chromosomal end protection. Rather, accessory proteins that interact with the shelterin complex are also essential for telomere stability. One such protein is SNM1B/Apollo, a member of a small gene family that also includes SNM1A and SNMIC/Artemis. All three proteins share sequence similarity to the yeast interstrand crosslink (ICL) repair protein PSO2/SNM1 (Dronkert *et al*, 2000). These proteins are characterized by a conserved metallo-β-lactamase-fold and an appended β-*C*PSF-*A*rtemis-*S*nm1-*P*so2 (CASP) domain that together imparts 5′ exonuclease function (Callebaut *et al*, 2002; Poinsignon *et al*, 2004; Lenain *et al*, 2006). SNM1A localizes to ionizing radiation (IR)-induced DNA breaks (Richie *et al*, 2002) and is involved in ATM-mediated G1 checkpoint after IR exposure (Akhter and Legerski, 2008) and mitotic checkpoint control (Akhter *et al*, 2004). Deletion of SNM1A in the mouse results in predisposition to infections and cancer, suggestive of functions in the maintenance of proper immune function and DNA repair (Ahkter *et al*, 2005). The SNM1C/Artemis nuclease functions in the opening of hairpins generated during VDJ recombination and also have a function in the repair of IR-induced DNA damage (Moshous *et al*, 2001; Ma *et al*, 2002; Rooney *et al*, 2003; Cabuy *et al*, 2005). In addition, SNM1C/Artemis also has a major function in mediating the regulation of the cell cycle in response to various forms of stress (Zhang *et al*, 2004, 2009; Geng *et al*, 2007; Wang *et al*, 2009). SNM1B/Apollo was originally found to have a function in ICL repair (Demuth *et al*, 2004; Bae *et al*, 2008) and functions in a mitotic checkpoint similar to SNM1A (Liu *et al*, 2009). SNM1B/Apollo has also been shown to be a telomere-binding protein through its interaction with TRF2 (Freibaum and Counter, 2006; Lenain *et al*, 2006; Chen *et al*, 2008; Demuth *et al*, 2008; van Overbeek and de Lange, 2006). The shRNA-mediated depletion of SNMIB/Apollo initiates the onset of a senescent phenotype because of the generation of a DDR at telomeres primarily at S-phase (van Overbeek and de Lange, 2006). Moreover, recent evidences indicate that TRF2 and Apollo relieve topological stress during telomere replication (Ye *et al*, 2010). Collectively, these data indicate

*Corresponding author. Department of Genetics Unit 1010, MD Anderson Cancer Center, 1515 Holcombe Boulevard, Box 1006, Houston, TX 77030, USA. Tel.: +1 713 834 6361; Fax: +1 713 834 6319; E-mail: schang@mdanderson.org
[6]Present address: Department Of Laboratory Medicine, Yale University School of Medicine, CB 403, 333 Cedar St., New Haven, CT 06520, USA

Received: 3 February 2010; accepted: 19 May 2010; published online: 15 June 2010

that SNMIB/Apollo have an important function in shielding telomeres from replicative damages. Interestingly, in human cells, siRNA-mediated knockdown of SNMIB/Apollo alone did not result in significant end-to-end chromosome fusions; a telomere fusion phenotype was obvious only when TRF2 was also removed, suggesting that SNMIB/Apollo also contributes to prevent the repair of chromosome ends by NHEJ (Lenain *et al*, 2006).

As earlier reports on the telomere functions of SNMIB/Apollo were based on RNA interference (RNAi)-mediated partial gene-knockdown approaches, the complete set of functions performed by SNM1B/Apollo at telomeres remains elusive. To address the function of mammalian SNM1B/Apollo at telomeres, we used a gene-targeting strategy to completely knockout SNMIB/Apollo function in the mouse genome. *SNMIB/Apollo* null mouse embryo fibroblasts (MEFs) exhibit a defect in the generation of 3′ ss overhangs and an increased incidence of chromatid-type fusions involving leading-strand telomeres, consistent with a function for SNMIB/Apollo in protecting leading-strand telomeres after DNA replication. We show that mutations within its conserved nuclease domain abolish this end-protective phenotype, suggesting that SNMIB/Apollo is a pivotal 5′–3′ exonuclease required for generation of the protective 3′ ss overhangs at leading-strand telomeres after DNA replication to prevent engagement of the NHEJ pathway.

Results

Generation of SNMIB/Apollo knockout mice

The murine *SNMIB/Apollo* locus contains four exons, with exon 1 containing the ATG start codon and exon 4 the stop codon. Exon 1 is located only 250 bp from AP-4b1, a gene that encodes a component of the *trans*-Golgi network that is likely to be important for normal cellular physiology (Dell'Angelica *et al*, 1999). To avoid perturbing this gene, we used a targeting strategy to delete exon 4 by replacing it with pGK-neo (Figure 1A). We inserted the pGK-neo gene in the opposite transcription orientation as the Apollo transcript, reasoning that any transcript originating from Apollo exon 1 would be disrupted by transcripts originating from the strong Neo promoter. In addition, in the unlikely event that transcription of exons 1–3 results in the generation of an aberrant protein product, deleting exon 4 would abolish its ability to localize to telomeres, as exon 4 contains the TRF2-interacting motif essential for Apollo's localization to telomeres (Chen *et al*, 2008; Freibaum and Counter, 2008). PCR analyses revealed that the correct recombination events occurred in two embryonic stem cell clones, F2 and D6 (Figure 1A and B). These clones were selected to generate chimeras and the genotypes of their offspring were determined by PCR (Figure 1C). We confirmed that an *SNMIB/Apollo* null allele was generated by showing that RT–PCR of total RNA isolated from E13.5 *SNMIB/Apollo*$^{-/-}$ MEFs failed to detect any *SNMIB/Apollo* transcripts encoding exon 4 (Figure 1D). In comparison, an shRNA-mediated knockdown approach resulted only in ~60% knockdown of *SNMIB/Apollo* transcripts (Figure 1D; Lenain *et al*, 2006). Deletion of *SNMIB/Apollo* resulted in a two-fold decline in cell growth, consistent with *SNMIB/Apollo* null cells experiencing a growth inhibiting DDR (Figure 1E). In agreement with this observation, increased accumulation of dysfunctional telomere-induced DDR foci (TIFs) (d'Adda di Fagagna *et al*, 2003; Takai *et al*, 2003) were observed in *SNMIB/Apollo* null MEFs. Compared with *SNMIB/Apollo* proficient MEFs, 37 ± 1.7% of *SNMIB/Apollo*$^{-/-}$ MEFs displayed four or more TIFs per nucleus (Figure 1F and G), consistent with a function for SNMIB/Apollo in protecting telomeres from activating a DDR. E13.5 *SNMIB/Apollo*$^{-/-}$ embryos were smaller than wild-type embryos, and 100% of *SNMIB/Apollo*$^{-/-}$ neonates die at postnatal day 0 (P0), indicating that *SNMIB/Apollo* is essential for normal murine development (Akhter *et al*, in preparation).

SNMIB/Apollo generates the 3′ overhang to protect leading-strand telomeres from inappropriate repair

Immediately after DNA replication, telomeres created by leading-strand DNA synthesis are expected to be initially blunt ended, whereas lagging-strand synthesis results in telomeres possessing a 3′ ss overhang, the extent of which is dependent on placement and removal of the terminal RNA primer and/or the action of 5′–3′ exonucleases. As SNMIB/Apollo mediates 5′–3′ exonuclease activity *in vitro* (Lenain *et al*, 2006), we investigated whether it might be required for 5′ end resection to generate the 3′ overhang. If SNM1B/Apollo is specifically involved in the 5′ resection of telomere ends after replication, its loss would result in a reduction in 3′ ss overhang intensity. However, total telomere length is not predicted to change. To test this hypothesis, we performed in-gel hybridization assay on immortalized wild-type, *SNMIB/Apollo*$^{-/+}$ and *SNMIB/Apollo*$^{-/-}$ MEFs to detect the 3′ ss telomeric overhang as well as total telomeric DNA. Compared with wild-type and heterozygous littermate controls, an ~65% reduction of telomere 3′ overhang signals was observed in two independently derived lines of *SNMIB/Apollo*$^{-/-}$ MEFs (Figure 2A). We also did not detect any change in total telomere length even in late passage MEFs (Supplementary Figure 1). These results suggest that SNMIB/Apollo has an important function in the generation of the 3′ ss overhang. It is worth noting that in human cells, a reduced expression of SNM1B/Apollo by RNAi does not trigger a loss of the 3′ overhang while telomere deprotection is apparent (van Overbeek and de Lange, 2006; Ye *et al*, 2010). This seeming dicrepancy might reflect either difference in the function of SNM1B/Apollo between mouse and human cells or the necessity to fully abrogate its expression to reveal its function in the regulation of the 3′ overhang length or both.

The generation of a 3′ ss G-rich overhang by SNMIB/Apollo in newly synthesized telomere ends is postulated to provide protection from NHEJ-mediated repair, as ss telomeric DNAs are poor substrates for this repair reaction (Deng *et al*, 2009). To test the hypothesis, we examined chromosome fusion events on metaphase spreads of control and *SNMIB/Apollo*$^{-/-}$ MEFs by telomere chromosome orientation-FISH (CO-FISH), which permits the differentiation between the telomeres generated by leading and lagging-strand DNA synthesis (Bailey *et al*, 2001). We found that 100% of *SNMIB/Apollo* null MEFs exhibited chromosome aberration with telomeric signals at sites of fusion (indicative of uncapped telomeres), comprising ~8% of all chromosome ends (Figure 2B–F). The majority of these telomere fusions were end-to-end chromosome fusions that have occurred either in the G1- or G2-phase of the cell cycle (Figure 2C and E). However, ~10% of these fusions bore hallmarks of telomere

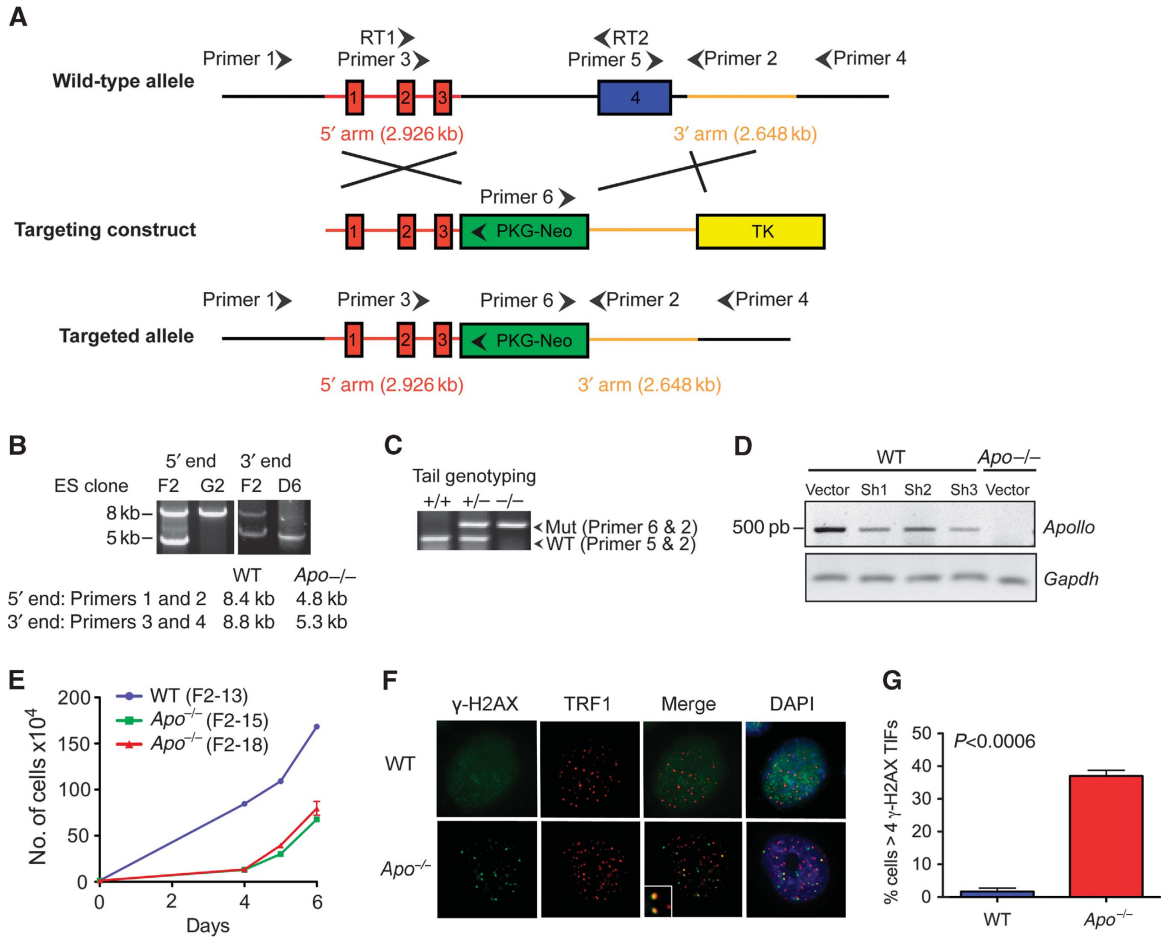

Figure 1 Generation of *Apollo* knockout mice. (**A**) Schematic representation of the endogenous *SNM1B/Apollo* allele, the targeting construct and the predicted structure of the mutant allele generated by homologous recombination. Transcriptional orientations of the SNM1/Apollo and the Pgk-neo genes are indicated, as are primers used for genotyping. (**B**) PCR analysis using the indicated primers was performed to screen for ES cells that underwent correct homologous recombination. Clones F2 and D6 were selected for blastocyst injection to generate *SNM1B/Apollo* heterozygous mouse. These mice were mated to obtain *SNM1B/Apollo* wild-type, heterozygous and null embryos (**C**). (**D**) RT–PCR using primer set RT1 and RT2 does not amplify *SNM1B/Apollo* mRNA transcript from total RNA isolated from *SNM1B/Apollo* null MEFs. shRNA generated against *SNM1B/Apollo* (sh1-3) reveal that the amplified band in WT MEF is specific to *SNM1B/Apollo* mRNA. (**E**) Growth curves of two independently derived *SNM1B/Apollo*$^{-/-}$ and wild-type SV40-immortalized MEFs. (**F**) Robust γ-H2AX TIF formation in SV40-immortalized *SNM1B/Apollo*$^{-/-}$ MEFs. Cells were co-stained with anti-TRF1 (red), anti-γ-H2AX (green) and DAPI (blue) for DNA. (**G**) Quantification for the frequency of γ-H2AX-positive TIFs observed in wild-type and *SNM1B/Apollo* null MEFs. Cells processed as described in (**F**) were scored for four or more telomeric γ-H2AX foci. Error bars: s.e.m., $n \geqslant 300$; $P < 0.006$ calculated using a two-tailed Student's *t*-test.

repair occurring exclusively in G2 (Figure 2C and E); chromatid-type fusions, characteristic of post-replicative repair in G2, were observed in the absence of SNMIB/Apollo, but not in wild-type cells (Figure 2D and F). If chromatid-type telomere fusions occurred randomly, a 1:2:1 ratio of leading–leading, leading–lagging and lagging–lagging telomere participation would be expected. Instead, CO-FISH analysis showed that >80% of chromatid-type fusions involved the end joining of two leading-strand telomeres, revealing preferential failure of end capping on leading-strand telomeres at or immediately after DNA replication and subsequent repair (Figure 2F). Fusion events involving lagging-strand telomeres were rare, with lagging–lagging, lagging–leading and sister–sister chromatid-type fusions being observed (Figure 2D and F). Chromosomes with multiple interstitial telomeric signals in long blocks throughout the chromosome arms were also found (Figure 2B); the nature of these aberrations is not clear at this time, but is likely to involve defects in telomere replication. Taken together, these results suggest that SNMIB/Apollo is required to protect leading-strand telomeres at or shortly after their replication by promoting formation of the protective 3′ ss overhang to prevent inappropriate repair in G2.

SNM1B/Apollo nuclease activity prevents NHEJ-mediated repair of dysfunctional telomeres

To determine whether the telomere fusions observed in *SNMIB/Apollo*$^{-/-}$ MEFs were mediated by the NHEJ pathway, we crossed *SNMIB/Apollo*$^{+/-}$ mice with *Ku70*$^{+/-}$ mice to generate *SNMIB/Apollo*$^{-/-}$*Ku70*$^{-/-}$ MEFs. In the absence of *Ku70*, a core NHEJ factor, chromosome- and chromatid-type telomere fusions, as a result of *SNMIB/Apollo* loss, were reduced by ~10- and ~3.5-fold, respectively (Figure 3A–C). These results are consistent with the NHEJ pathway as the major repair pathway of uncapped telomeres in *SNMIB/Apollo* null MEFs.

SNMIB/Apollo exhibits 5′–3′ DNA exonuclease activity *in vitro* that favours double-stranded DNA substrates with a

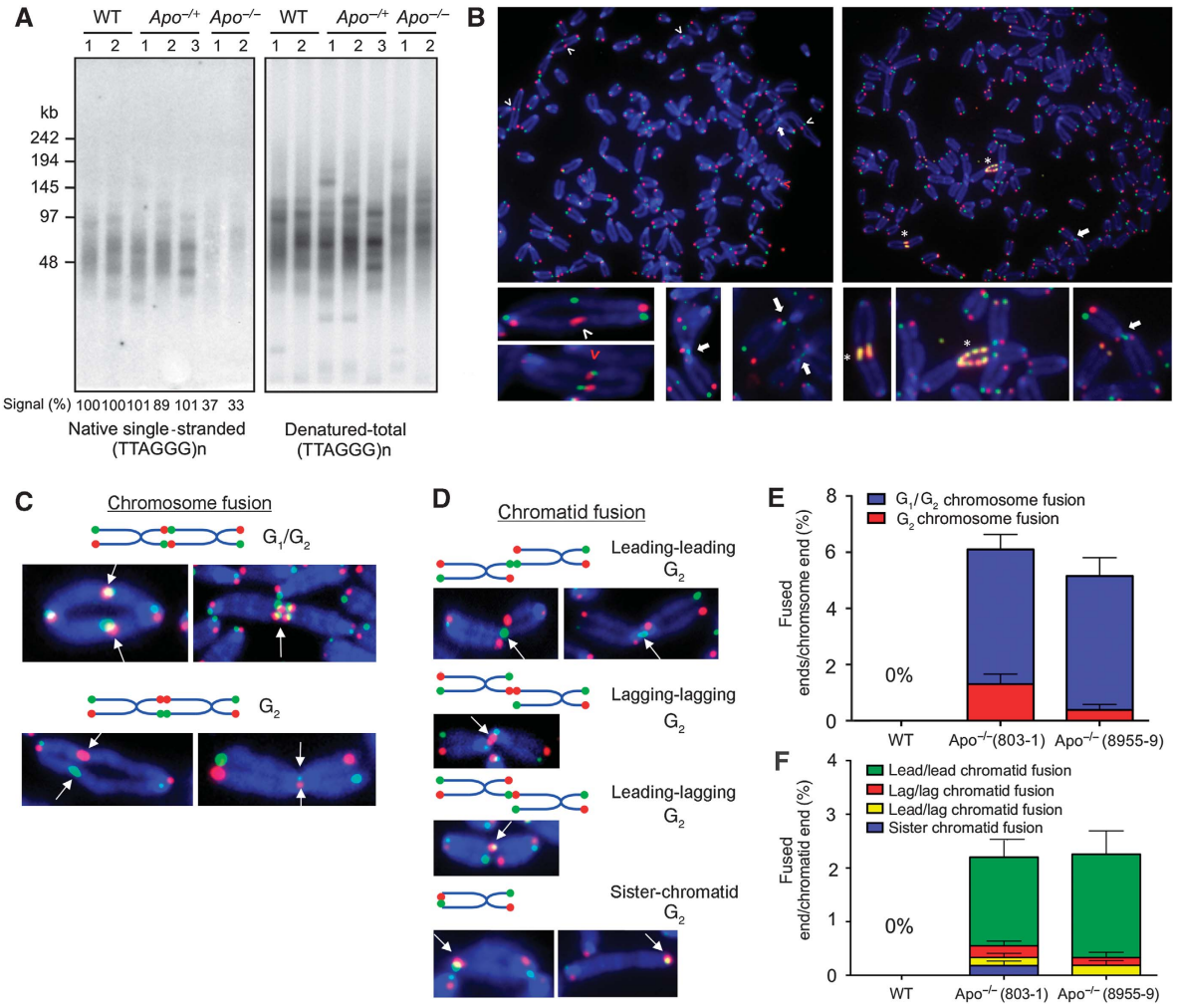

Figure 2 Characterization of *SNM1B/Apollo*$^{-/-}$ MEFs. (**A**) In-gel hybridization assay using a CHEF gel to fractionate *SNM1B/Apollo*$^{-/-}$, *SNM1B/Apollo*$^{+/-}$ and wild-type MEFs DNA (two to three independent lines per genotype), then hybridized *in situ* to a $(CCCTAA)_4$ probe to detect the 3′ overhang under native conditions and under denatured conditions to detect total TTAGGG repeats. Overhang signals were quantified with ImageJ software and normalized to the total telomeric signal of the same lane. The numbers below the gel represent the percentage of normalized overhang signal compared with the normalized overhang signal of wild-type MEFs (#1), which is arbitrarily set as 100%. (**B**) Chromosomal aberrations in *SNM1B/Apollo*$^{-/-}$ MEFs. Representative metaphase spreads of *SNM1B/Apollo*$^{-/-}$ MEFs. Arrows: leading–leading-strand chromatid fusions; white arrowheads: G2 chromosome fusions; red arrowheads: G1/G2 chromosome fusions; asterisk: chromosomes with multiple interstitial telomeric signals. (**C**) Schematic and examples of chromosome-type fusions observed in *SNM1B/Apollo*$^{-/-}$ MEFs. Green: FITC-OO-$(TTAGGG)_4$ probe detects the leading strand; red: TAMRA-OO-$(CCCTAA)_4$ detects the lagging strand; blue: DAPI detects DNA. Arrows point to fusion sites. (**D**) Schematic and examples of chromatid-type and sister–sister telomere fusions observed in *SNM1B/Apollo*$^{-/-}$ MEFs. Arrows point to fusion sites. (**E**) Quantification of chromosome-type fusions of wild-type and *SNM1B/Apollo*$^{-/-}$ MEFs. Error bars: s.e.m. (**F**) Quantification of chromatid-type and sister fusions of wild-type and *SNM1B/Apollo*$^{-/-}$ MEFs. Error bars: s.e.m.

3′ overhang (Lenain *et al*, 2006). Sequence alignment of SNMIB/Apollo with SNM1 and Artemis revealed the presence of a metallo-β-lactamase-fold and a β-CASP domain (Figure 3D; Supplementary Figure 2). The β-CASP domain is a nucleic acid-binding domain, and together with the metallo-β-lactamase hydrolase has been shown to constitute a nuclease function for SMN1 family members (Ma *et al*, 2002; Pannicke *et al*, 2004; Li *et al*, 2005; Lenain *et al*, 2006; Hazrati *et al*, 2008). Recent data revealed that mutating the conserved amino-acid residues D14 and D35 to glutamine completely abolished the human SNM1B/Apollo exonuclease activity *in vitro* (Ye *et al*, 2010). Here, we confirm these results by showing that mutating D14, D35 and D145 to alanine also abolishes the SNM1B/Apollo exonuclease activity *in vitro* (Supplementary Figure 3). To determine whether the nuclease function of SNMIB/Apollo is required to protect telomeres from engaging in NHEJ-mediated repair reactions, we used a mutant that deleted the conserved FLxHxHxDHxxGL nuclease domain (SNMIB/Apollo$^{\Delta 28-40}$) and the SNMIB/Apollo^{D14A} exonuclease-dead point mutant (Figure 3D; Supplementary Figures 2 and 3). After establishing that these mutants localized to telomeres by indirect immunofluorescence (Supplementary Figure 4A and B), we examined the impact of the reconstituted proteins on the number of chromosome fusions generated. We reasoned that if SNM1B/Apollo nuclease activity is required to protect leading-strand telomeres, then expressing wild-type but not mutant *SNM1B/Apollo* constructs will reduce the number of chromosome fusions observed. However, because of the high rate of background chromosome fusions in *SNM1B/Apollo* null MEFs, it was difficult to determine whether SNM1B/Apollo constructs had any function on chromosome fusion formation. Instead,

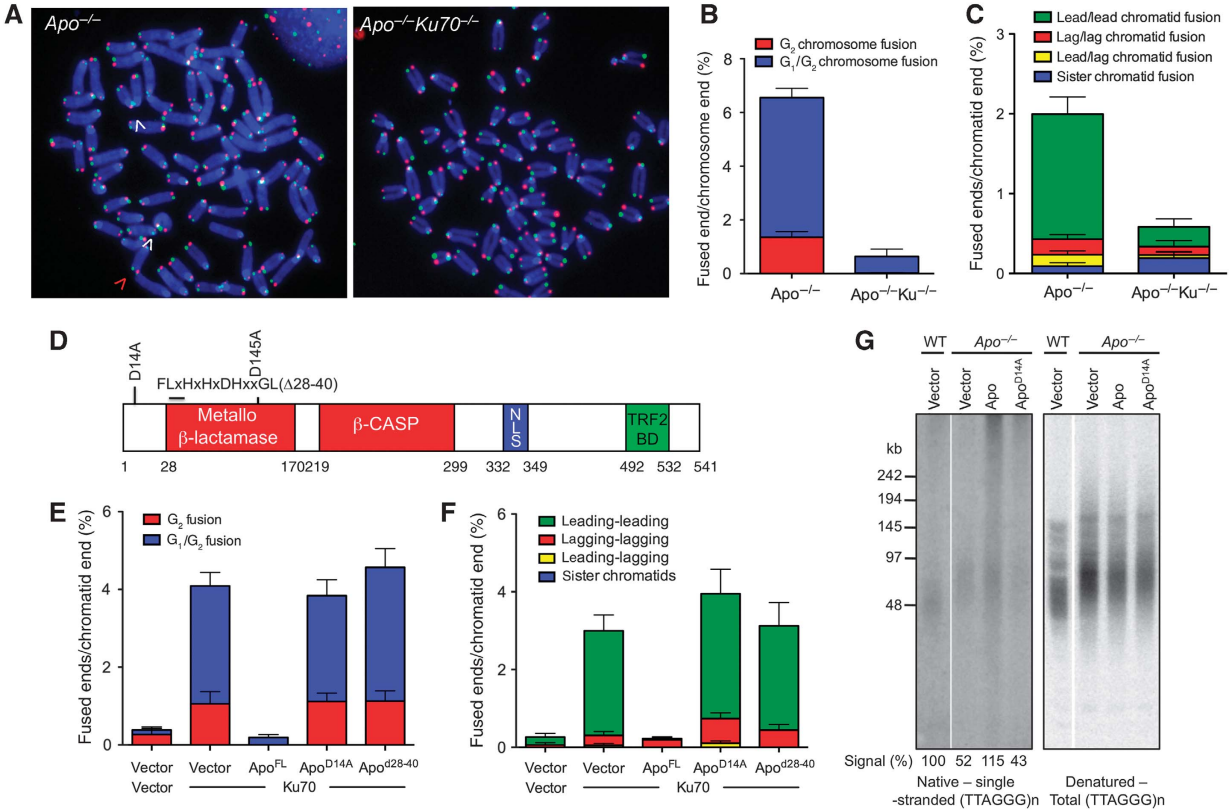

Figure 3 SNM1B/Apollo nuclease activity is required to prevent NHEJ-mediated repair of dysfunctional telomeres. (**A**) CO-FISH analysis of metaphase spreads of *SNM1B/Apollo*$^{-/-}$ and *SNM1B/Apollo*$^{-/-}$*Ku70*$^{-/-}$ MEFs (green: FITC-OO-$(TTAGGG)_4$ probe detects the leading strand; red: TAMRA-OO-$(CCCTAA)_4$ detects the lagging strand. White arrowheads: leading–leading chromatid fusions; red arrowheads: leading–lagging chromatid fusions. Quantification of chromosome-type fusions (**B**) and chromatid–chromatid fusions (**C**) observed in (**A**). Error bars: s.e.m. (**D**) Schematic of SNMIB/Apollo constructs generated with the indicated point mutation or deletion. Quantification of chromosome-type fusions (**E**) and chromatid-type and sister fusions (**F**) observed in *SNM1B/Apollo*$^{-/-}$*Ku70*$^{-/-}$-deficient MEFs reconstituted with the indicated SNM1B/Apollo mutants and Ku70 or vector DNA. Error bars: s.e.m. (**G**) In-gel hybridization assay using a CHEF gel to fractionate DNA isolated from *SNM1B/Apollo*$^{-/-}$ and wild-type MEFs reconstituted with the indicated SNM1B/Apollo constructs, then hybridized to a $(CCCTAA)_4$ probe to detect the 3′ overhang under native conditions (left) and under denatured conditions (right) to detect total TTAGGG repeats. Overhang signals are normalized to the total telomeric signal of the same lane. The relative overhang signals were obtained by comparing the percentage of normalized overhang signal of each condition to the normalized overhang signal of wild type plus vector control, which is arbitrarily set as 100%.

we reconstituted wild-type and mutant *SNM1B/Apollo* constructs in *SNMIB/Apollo*$^{-/-}$*Ku70*$^{-/-}$ MEFs. In the absence of *Ku70*, very few background chromosome fusions were observed in *SNMIB/Apollo* MEFs (Figure 3E and F). When the Ku70 cDNA was reintroduced into these cells, we observed that reconstitution of wild-type SNMIB/Apollo almost completely eliminated end-to-end chromosome fusions and leading–leading chromatid-type fusions (Figure 3E and F). In sharp contrast, extensive chromosome and chromatid fusions were observed in both the SNMIB/Apollo$^{\Delta 28-40}$ and the SNMIB/Apollo^{D14A} mutants (Figures 3E and F). Finally, we examined the status of the 3′ ss overhang in *SNMIB/Apollo*$^{-/-}$ MEFs reconstituted with vector, wild-type SNMIB/Apollo or the nuclease-defective SNMIB/Apollo^{D14A} mutant by the in-gel hybridization assay. *SNMIB/Apollo* null MEF expressing the SNMIB/Apollo^{D14A} mutant was not able to efficiently generate the 3′ ss overhang, and only introduction of wild-type SNMIB/Apollo restored the 3′ overhang to levels observed in wild-type MEFs (Figure 3G). Taken together, these data suggest that the nuclease function of SNMIB/Apollo is crucial for the formation of functional telomeres and protection of chromosome ends from aberrant NHEJ-mediated repair.

Tpp1–Pot1a/b cooperates with SNM1B/Apollo to protect leading- and lagging-strand telomeres from NHEJ-mediated repair

Removal of Trf2 from telomeres induces a DDR that preferentially activates ATM, whereas removal of the Tpp1–Pot1a/b complex activates an ATR-dependent DDR (Denchi and de Lange, 2007; Guo *et al*, 2007; Deng *et al*, 2009). These results suggest that the respective losses of Trf2 and Tpp1–Pot1a/b might result in the activation of distinct repair processes at telomeres. We, therefore, compared how depletion of these two shelterin components affects the telomere repair phenotypes in the setting of *SNM1B/Apollo* deficiency. We uncapped telomeres in SV40LT-immortalized *SNM1B/Apollo* null MEFs by efficiently depleting endogenous Trf2 or Tpp1 using retrovirus-mediated short hairpin RNA (Deng *et al*, 2009). Although depletion of Tpp1 in wild-type cells resulted in chromosome fusions involving ~10% of chromosome ends, removal of Tpp1 from *SNM1B/Apollo*$^{-/-}$ MEFs led to a six-fold increase in the number of fused chromosomes to involve ~60% of all ends (Figure 4A and B). In contrast, depletion of Trf2 in *SNM1B/Apollo*-deficient MEFs increased chromosome fusions by only 20% over wild-type MEFs

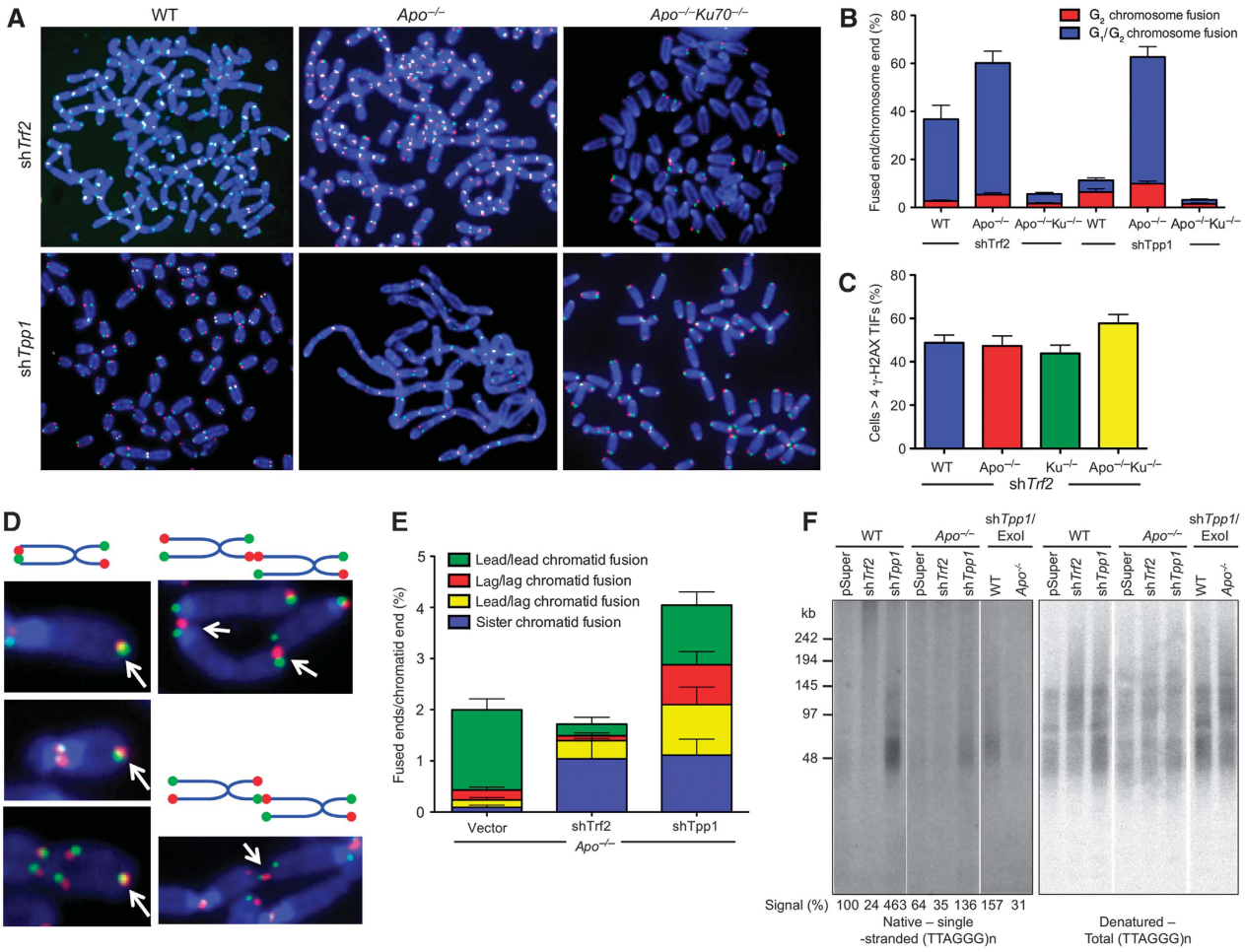

Figure 4 Tpp1–Pot1a/b protects telomeres of SNM1B/Apollo null MEFs from NHEJ-mediated repair. (**A**) CO-FISH analysis of metaphase spreads of wild-type, *SNM1B/Apollo*$^{-/-}$ and *SNM1B/Apollo*$^{-/-}$*Ku70*$^{-/-}$ MEFs treated with either shTrf2 or shTpp1, as indicated. Green: FITC-OO-$(TTAGGG)_4$ probe detects the leading strand; red: TAMRA-OO-$(CCCTAA)_4$ detects the lagging strand. (**B**) Quantification of chromosome-type fusions observed in (**A**). Error bars: s.e.m. (**C**) Quantification of γ-H2AX positive TIFs in SV40-LT-immortalized MEFs of the indicated genotypes expressing shTrf2. Cells were harvested 72 h after infection and processed for IF-FISH. For each genotype, a minimum of 200 cells were scored for four or more telomeric γ-H2AX foci. Error bars: s.e.m. (**D**) Schematic and examples of sister telomere and lagging-strand chromatid-type fusions observed in *SNM1B/Apollo*$^{-/-}$ MEFs expressing shTpp1. Arrows point to fusion sites. (**E**) Quantification of chromatid-type and sister fusions observed in *SNM1B/Apollo*$^{-/-}$ MEFs expressing either vector control, shTrf2 or shTpp1. Error bars: s.e.m. (**F**) In-gel hybridization assay using a CHEF gel to fractionate DNA isolated from *SNM1B/Apollo*$^{-/-}$ and wild-type MEFs after removal of Trf2 or Tpp1. $(CCCTAA)_4$ probe was used to detect the 3′ overhang under native conditions (left) and under denatured conditions (right) to detect total TTAGGG repeats. Overhang signals were quantified with ImageJ software and normalized to the total telomeric signal of the same lane. The relative overhang signals were obtained by comparing the percentage of normalized overhang signal of each condition to the normalized overhang signal of wild type retrovirally infected with empty vector, which is set as 100%. ExoI: Exonuclease I.

(Figure 4A and B). This surprising result suggests that the Tpp1–Pot1a/b complex cooperates with SNM1B/Apollo to protect telomeres from engaging NHEJ-mediated repair, and supports our earlier observation that the Tpp1–Pot1a complex protects telomeres from inappropriate repair as well as Trf2 (Deng *et al*, 2009). We found that both *Trf2* and *Tpp1*-depleted telomeres were not repaired (fused) in *SNMIB/Apollo*$^{-/-}$*Ku70*$^{-/-}$ MEFs, suggesting that these chromosome fusions take place through NHEJ-mediated repair (Figure 4A and B). These 'unrepaired' telomeres remain dysfunctional, as indicated by robust accumulation of γ-H2AX at telomeres (Figure 4C; Supplementary Figure 5).

Although the majority of chromatid-type telomere fusion observed in *SNMIB/Apollo*$^{-/-}$ MEFs involved leading-strand telomeres, a small percentage of lagging–lagging, lagging–leading and sister–sister (lagging–leading) were also observed (Figure 2F). This observation suggests that some lagging-strand telomeres also become uncapped in *SNMIB/Apollo*$^{-/-}$ MEFs. The enhanced telomere protection phenotype observed between Tpp1–Pot1a/b and SNM1B/Apollo suggests that Tpp1–Pot1a/b is required to protect telomeres processed by SNM1B/Apollo. We postulate that the lagging-strand 3′ ss overhang might be quickly bound and protected by the Tpp1–Pot1a/b complex after DNA replication. For the leading-strand telomere, it is likely that similar protection by Tpp1–Pot1a/b occurs after exonuclease digestion of the 5′ strand and generation of a 3′ ss overhang. Therefore, we reasoned that removal of Tpp1–Pot1a/b should result in increased uncapping of both lagging- and leading-strand telomeres, and thus increase the number of chromatid-type fusions involving both leading- and lagging-strand telomeres. Indeed, removal of Tpp1 from *SNMIB/Apollo*$^{-/-}$ MEFs resulted in telomere deprotection, apparent from the accumulation of γ-H2AX at telomeres (Supplementary Figure 6A and B).

We observed chromatid-type lagging–lagging, leading–leading and lagging–leading fusions at a ratio of ~1:1:1 in *SNMIB/Apollo*$^{-/-}$ MEFs devoid of Tpp1–Pot1a/b, suggesting uncapping of both leading- and lagging-strand telomeres (Figure 4D and E). We also monitored the formation of sister–sister chromatid-type fusions (i.e. sister union), as these represent obligate fusions between leading- and lagging-strand telomeres, allowing us to examine the integrity of both leading- and lagging-strand telomeres. A 12-fold increase in the number of sister–sister fusions was observed in *SNMIB/Apollo*$^{-/-}$ MEFs when Tpp1 was depleted from telomere ends, suggesting that the Tpp1–Pot1a/b complex is required to protect both leading- and lagging-strand telomeres from NHEJ-mediated repair in G2 (Figure 4E). We also observed an increase in sister–sister telomere fusions, but not other chromatid-type lagging-strand telomere fusions, when Trf2 was depleted in *SNMIB/Apollo*$^{-/-}$ MEFs, in agreement with earlier published results (Smogorzewska *et al*, 2002).

Finally, we examined the status of the 3′ ss overhang in *SNMIB/Apollo*$^{-/-}$ MEFs. As expected, removal of Trf2 from wild-type MEFs resulted in a decrease in overhang intensity that correlated with the increase in telomere fusion (Figure 4F). In contrast, removal of Tpp1 resulted in dramatic overhang extension because of unrestrained telomerase activity at telomeres (Figure 4F) (Wang *et al*, 2007; Xin *et al*, 2007). However, it is also possible that Tpp1–Pot1a/b regulates a 5′–3′ exonuclease to prevent unregulated nucleolytic processing. In this scenario, depletion of Tpp1 would result in unrestrained nucleolytic activity at the 5′ end of the leading strand, contributing to increased overhang formation. To examine whether SNM1B/Apollo is this exonuclease, we depleted Tpp1–Pot1a/b in *SNM1B/Apollo* null MEFs. In shTpp1-treated *SNMIB/Apollo*$^{-/-}$ MEFs, overhang intensity was reduced ~3.3-fold, suggesting that SNM1B/Apollo does contribute to overhang formation observed after Tpp1–Pot1a/b loss. Taken together, these results suggest that Tpp1–Pot1a/b is required to protect newly synthesized leading- and lagging-strand telomeres from DNA repair. In the absence of SNM1B/Apollo, removal of Tpp1–Pot1a/b results in telomere fusions as robust as those observed when Trf2 is removed from telomeres, suggesting that the Tpp1–Pot1a/b complex could efficiently protect telomeres from engaging DNA repair pathways. Our results also suggest that Tpp1–Pot1a/b regulates SNM1B/Apollo nuclease activity at the leading strand.

SNM1B/Apollo nuclease activity suppresses chromosome fusions induced by telomere uncapping

As depletion of Trf2 or Tpp1–Pot1a/b in *SNM1B/Apollo*$^{-/-}$ MEFs resulted in robust chromosome fusions, we asked whether the nuclease activity of SNM1B/Apollo is required to provide protection from NHEJ-mediated repair in these settings. As expression of shTrf2 resulted in a very high rate of telomere fusions even in the wild-type MEFs, we used a dominant-negative form of TRF2, TRF2$^{\Delta B\Delta M}$, which results in a milder fusion phenotype. In accordance with what has been observed in human cells (Lenain *et al*, 2006; Ye *et al*, 2010), *SNM1B/Apollo*$^{-/-}$ MEFs expressing TRF2$^{\Delta B\Delta M}$ displayed an increase in the number of end-to-end chromosome fusions that involve 30% of chromosome ends as compared with 7% of ends for wild-type MEFs (Figure 5A and B). Expression of wild-type SNMIB/Apollo cDNA in this setting reduced the number of chromosome fusions by 5.5-fold (Figure 5B). In contrast, the nuclease-defective SNMIB/Apollo^{D14A} mutant was unable to suppress telomere fusions (Figure 5A and B). Consistent with earlier findings (Bailey *et al*, 2001), we also observed that overexpression of TRF2$^{\Delta B\Delta M}$ resulted in an increase in leading–leading chromatid-type fusions (Figure 5C). These chromatid fusions were reduced ~3-fold in *SNMIB/Apollo*$^{-/-}$ MEFs expressing wild-type SNMIB/Apollo, but not in *SNMIB/Apollo*$^{-/-}$ MEFs expressing the SNMIB/Apollo^{D14A} mutant (Figure 5C).

Similar to shRNA-mediated knockdown of Tpp1, expression of a dominant-negative form of Tpp1, Tpp1$^{\Delta RD}$, in wild-type cells resulted in minimal end-to-end telomere fusions (Guo *et al*, 2007). However, expression of Tpp1$^{\Delta RD}$ in *SNMIB/Apollo*$^{-/-}$ MEFs led to robust telomere fusions involving ~50% of chromosome ends (Figure 5D and E). Reconstitution of wild-type SNMIB/Apollo, but not the nuclease-dead SNMIB/Apollo^{D14A} mutant, in *SNMIB/Apollo*$^{-/-}$ MEFs reduced the number of chromosome- and chromatid-type leading–leading telomere fusions by four- and two-fold, respectively (Figure 5D–F). Taken together, these results reinforce the observation that SNMIB/Apollo's nuclease function is essential to mediate telomere end protection.

Repair of uncapped telomeres in SNMIB/Apollo null MEFs occurs independently of ATM function

Telomere uncapping resulting from the removal of TRF2 activates an ATM-dependent DDR, resulting in processing and repair of dysfunctional telomere ends by NHEJ primarily in G1 (Denchi and de Lange, 2007; Konishi and de Lange, 2008). To investigate the mechanism of repair of uncapped telomeres in *SNMIB/Apollo*$^{-/-}$ MEFs, we asked whether the ATM pathway is required to mediate chromosome end joining. We crossed *SNM1B/Apollo*$^{+/-}$ mice with *ATM*$^{+/-}$ mice to generate double heterozygous mice, and then crossed these to produce *SNMIB/Apollo*$^{-/-}$*ATM*$^{-/-}$ MEFs. In contrast to shRNA-mediated depletion of *Trf2* from telomeres of *ATM*$^{-/-}$ MEFs, in which γ-H2AX-positive TIF formation is largely abrogated, removal of Trf2 from *SNMIB/Apollo*$^{-/-}$ *ATM*$^{-/-}$ MEFs resulted in robust TIF formation (Supplementary Figure 6A and B). Surprisingly, telomere fusions were not abrogated in *SNMIB/Apollo*$^{-/-}$*ATM*$^{-/-}$ MEFs. Telomere fusions involving ~6% of chromosome ends were observed in these cells, comparable with the fusions observed in *SNMIB/Apollo*$^{-/-}$ MEFs (Figure 6A and B). Chromatid-type leading–leading telomere fusions in *SNMIB/Apollo*$^{-/-}$*ATM*$^{-/-}$ MEFs were also comparable with those observed in *SNMIB/Apollo*$^{-/-}$ MEFs (1.7% versus 1.9%, respectively). These results suggest that repair of telomeric ends in the absence of *SNMIB/Apollo* does not require functional ATM. When *Trf2* was depleted from *SNMIB/Apollo*$^{-/-}$*ATM*$^{-/-}$ MEFs, end-to-end telomere fusions involving ~40% of chromosome ends were observed, reinforcing the notion that efficient NHEJ-mediated repair of Trf2-depleted telomeres in the absence of *SNMIB/Apollo* occurs independent of ATM function (Figure 6D and E). Compared with shTrf2-treated *SNMIB/Apollo*$^{-/-}$ MEF, chromatid-type leading–leading telomere fusions increased ~15-fold in *SNMIB/Apollo*$^{-/-}$*ATM*$^{-/-}$ MEFs devoid of Trf2 (Figure 6F). Restoration of wild-type *SNMIB*/Apollo function, but not the nuclease-dead D14A mutant, in *SNMIB/Apollo*$^{-/-}$*ATM*$^{-/-}$ MEFs reduced both chromatid and chromosome fusions to

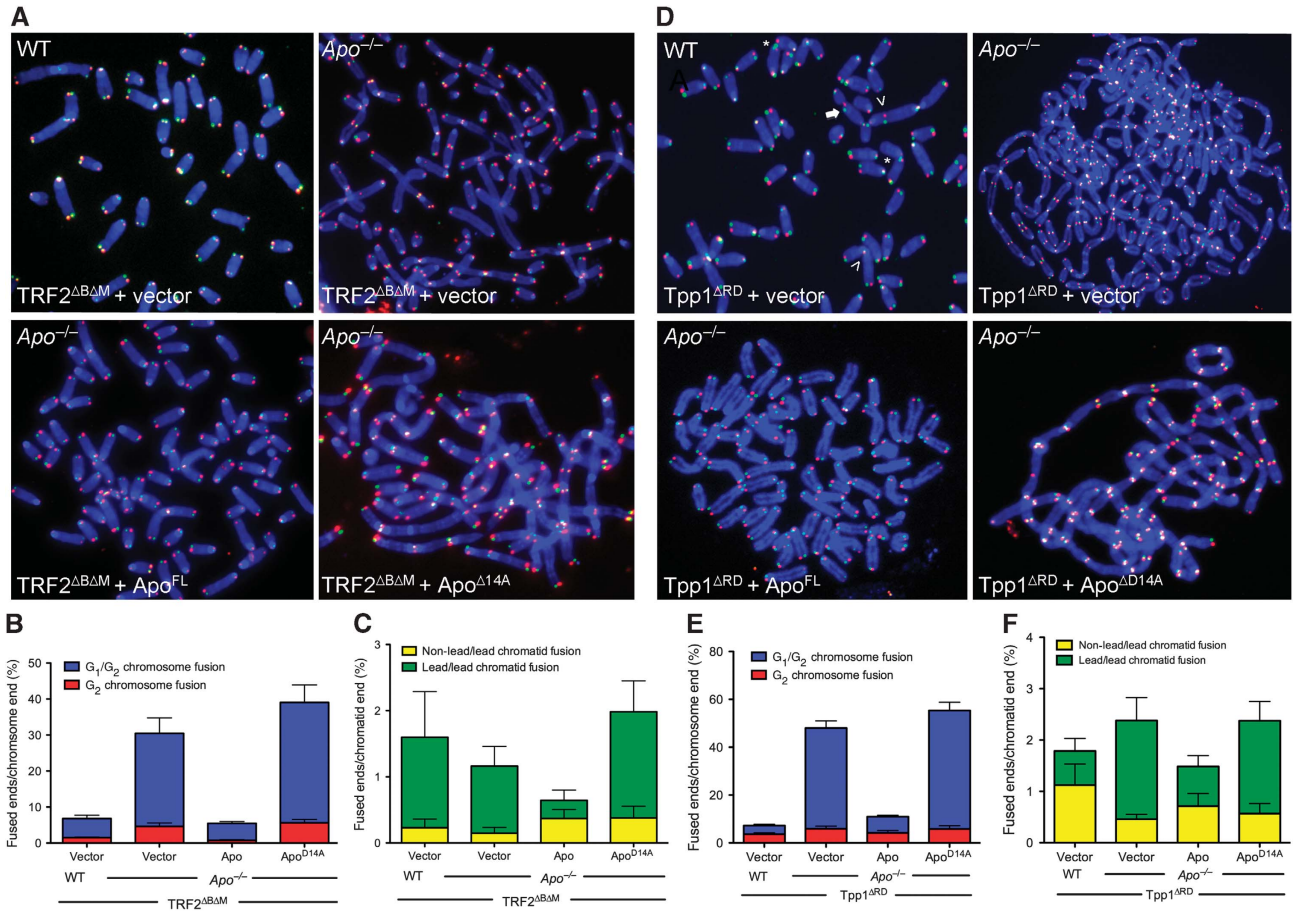

Figure 5 SNM1B/Apollo nuclease activity is required to suppress TRF2$^{\Delta B\Delta M}$ and TPP1$^{\Delta RD}$-induced telomere dysfunction. (**A**) Representative metaphase spreads of *SNM1B/Apollo*$^{-/-}$ MEFs expressing TRF2$^{\Delta B\Delta M}$ and reconstituted with the indicated SNM1B/Apollo constructs and analysed by CO-FISH. Green: FITC-OO-$(TTAGGG)_4$ probe detects the leading strand; red: TAMRA-OO-$(CCCTAA)_4$ detects the lagging strand. Quantification of chromosome-type (**B**) and chromatid-type (**C**) fusions observed in (**A**). Error bars: s.e.m. (**D**) Representative metaphase spreads of *SNM1B/Apollo*$^{-/-}$ MEFs expressing the Tpp1$^{\Delta RD}$ and reconstituted with the indicated SNM1B/Apollo constructs and analysed by CO-FISH. Green: FITC-OO-$(TTAGGG)_4$ probe detects the leading strand; red: TAMRA-OO-$(CCCTAA)_4$ detects the lagging strand. Quantification of chromosome-type (**E**) and chromatid-type (**F**) fusions described in (**D**). Error bars: s.e.m.

background levels (Figure 6G–I). Taken together, these results suggest that SNM1B/Apollo's nuclease function is required to protect newly replicated telomeres from engaging in ATM-dependent NHEJ. In the absence of SNM1B/Apollo, deprotected telomeres are efficiently repaired independent of ATM function during the G2-phase of the cell cycle.

Discussion

In this report, we show that SNM1B/Apollo has a pivotal function in protecting newly replicated leading-strand telomeres from NHEJ-mediated repair. We used a conventional mouse knockout approach to generate a null allele of *SNM1B/Apollo*. The growth defects, telomere dysfunction and chromosome/chromatid fusion phenotypes observed in our *SNM1B/Apollo*$^{-/-}$ MEFs could all be rescued by complementation with wild-type *SNM1B/Apollo* cDNA, therefore, showing that we have indeed generated a null allele of *SNM1B/Apollo*.

SNM1B/Apollo$^{-/-}$ MEFs display prominent chromatid-type fusions involving leading-strand telomeres, suggesting that in the absence of SNM1B/Apollo, NHEJ-mediated repair preferentially targets leading-strand telomeres shortly after synthesis. As telomeres fashioned by leading-strand DNA synthesis are supposed to be initially blunt ended, we propose that SNM1B/Apollo nuclease activity is required to generate the protective 3′ ss overhang (Figure 7). In support of this notion, reconstitution with wild-type, but not SNM1B/Apollo nuclease-defective mutants resulted in the formation of the 3′ ss overhang and rescued the leading-strand telomere chromatid-type fusion phenotype. Our data suggest that SNMIB/Apollo nuclease activity is required for 5′ end resection of the C-rich strand to generate sufficient 3′ ss overhang at leading-strand telomeres, thereby effectively repressing NHEJ of telomeres in G2. This processing step may, therefore, represent an essential prerequisite before the establishment of the t-loop structure postulated to participate in telomere-end protection.

SNM1B/Apollo and telomere-end protection in G2

Unlike lower eukaryotes, which primarily use homologous recombination (HR) to repair double-strand breaks (DSBs) and uncapped telomeres in G2, mammalian cells use NHEJ-mediated repair of DSBs efficiently throughout the cell cycle (Haber, 2000; Ferreira and Cooper, 2001; Lieber *et al*, 2003; Ferreira *et al*, 2004; Hartlerode and Scully, 2009). As all telomeric sequences are oriented in a 5′–3′ direction, end-to-end chromosome fusion could be generated only through

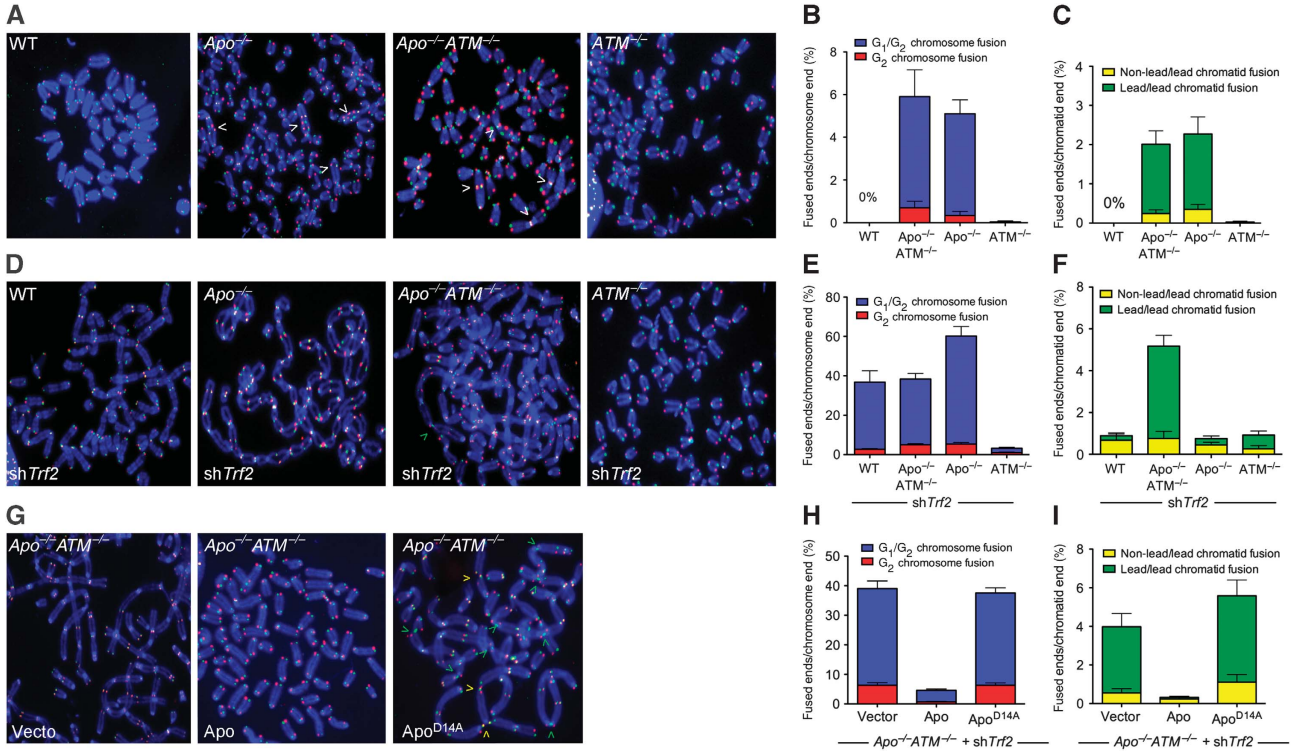

Figure 6 SNM1B/Apollo protects telomere fusions in G2 independent of ATM. (**A**) Metaphase spreads of SV40-LT-immortalized MEFs of indicated genotypes analysed by CO-FISH. Green: telomeric leading-strand DNA; red: telomeric lagging-strand DNA. White arrowheads indicate chromosome-type fusions. (**B**) Quantification of chromosome-type fusions described in (**A**). Error bars: s.e.m. (**C**) Quantification of chromatid-type fusions described in (**A**). Error bars: s.e.m. (**D**) Representative metaphase spreads of indicated genotypes after retroviral infection of shTRF2 for 120 h. Green arrowhead indicates the leading–leading chromatid fusion (**E**) Quantification of chromosome-type fusions described in (**D**). Error bars: s.e.m. (**F**) Quantification of chromatid-type fusions described in (**D**). Error bars: s.e.m. (**G**) Metaphase spreads of *SNM1B/Apollo*$^{-/-}$*ATM*$^{-/-}$ MEFs sequentially infected with retrovirus carrying shTRF2 and indicated SNM1B/Apollo constructs. Green arrowheads indicate the leading–leading chromatid fusions and yellow arrowheads indicate leading–lagging chromatid fusions. Quantification of chromosome-type (**H**) and chromatid-type fusions (**I**) described in (**G**). Error bars: s.e.m.

some form of NHEJ-mediated process and not through HR. Robust telomere fusion involving ~60% of chromosome ends were observed in *SNM1B/Apollo* null cells after removal of Trf2. Previous reports have suggested that mammalian telomeres deficient in Trf2 are primarily repaired in G1 (Figure 7) (Smogorzewska *et al*, 2002; Konishi and de Lange, 2008). However, another story and several lines of evidence presented here suggest that a significant fraction, if not all, of the telomere fusions observed in *Trf2*-depleted *SNM1B/Apollo* null MEFs were repaired in G2 (Bailey *et al*, 2001). First, ~10% of these telomere fusions possessed distinct hallmarks of G2 repair; that is they were of the G2 chromatid type, indicating that they formed at or shortly after replication. Second, although the majority of telomere fusions were of the chromosome type, suggestive of formation in G1, it is important to appreciate that these cells were cycling, so this pattern of fusion signals could also arise through segregation of chromatid-type telomere fusion (which occurred in G2) and replication in the next cell cycle. Third, the ATM pathway, while absolutely required to repair *Trf2*-deficient telomeres in G1, is completely dispensable for repair of uncapped telomeres and their resultant fusion observed in *SNM1B/Apollo*$^{-/-}$ MEFs lacking Trf2 (Figure 7). Indeed, the number of fused telomeres observed in *SNM1B/Apollo*$^{-/-}$*ATM*$^{-/-}$ MEFs is comparable with those observed in *SNM1B/Apollo*$^{-/-}$*ATM* wild-type MEFs. Together, these results argue that repair of uncapped telomeres in *SNM1B/Apollo*$^{-/-}$ MEFs takes place primarily in G2, after DNA replication, in an ATM-independent manner. Our results support a recent report documenting that the majority of IR-induced DSBs in human fibroblasts are repaired by NHEJ in G1 and G2 independent of ATM function (Beucher *et al*, 2009).

Tpp1–Pot1a/b protects newly synthesized single-strand overhangs from NHEJ-mediated repair

Immediately after DNA replication, newly replicated telomeres are recognized as DSBs to enable obligatory modification (Verdun *et al*, 2005). We postulate that newly replicated, blunt-ended leading-strand telomeres recruit DNA repair/processing factors, including the Mre11–Rad50–Nbs1 (MRN) complex (Attwooll *et al*, 2009; Deng *et al*, 2009; Dimitrova and de Lange, 2009) and SNM1B/Apollo, to initiate end resection of the C-strand. In contrast, the lagging-strand telomere possesses at least some length of 3′ ss overhang after replication and degradation of the terminal RNA primer required for Okazaki fragment initiation. It is also likely that the newly generated leading- and lagging-strand 3′ ss overhangs are immediately protected by binding of the Tpp1–Pot1a/b complex, thereby preventing engagement of the NHEJ pathway and extinguishing the DDR at telomeres. This scenario is analogous to RPA binding to newly resected DSBs possessing ss DNA ends; except in this context, the DDR is enhanced (Miyazaki *et al*, 2004). In support of this notion,

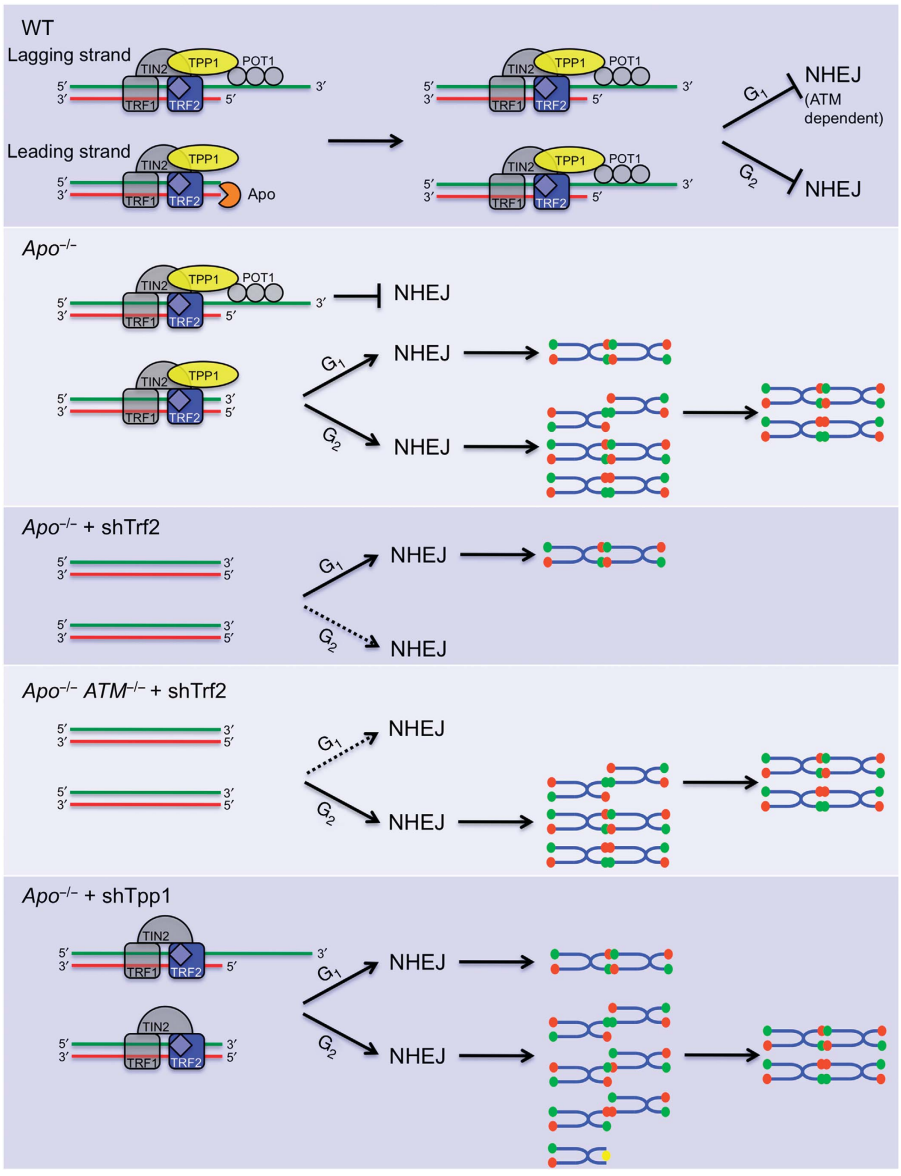

Figure 7 Speculative model for the function of SNM1B/Apollo at functional and uncapped telomeres. See text for details.

depletion of Tpp1 in *SNM1B/Apollo* null MEFs resulted in deprotection of both the leading and lagging strands, manifested as elevated numbers of chromatid-type fusions involving the lagging-strand telomere, including sister–sister telomere fusion (Figures 4D, E and 7E). Our observation of massive telomere fusions in Tpp1-depleted *SNM1B/Apollo* null MEFs was surprising, considering that these cytogenetic aberrations are never observed in either Pot1a or Tpp1 singly depleted MEFs (Hockemeyer *et al*, 2006; Wu *et al*, 2006; Guo *et al*, 2007). These results suggest that the presence of Trf2 is not sufficient to avert NHEJ-mediated telomere fusions when Tpp1–Pot1a/b is removed from telomeres in the setting of *SNM1B/Apollo* deficiency, and further supports our earlier data that under certain conditions, the Tpp1–Pot1a/b complex is able to efficiently protect telomeres from NHEJ-mediated repair independent of Trf2 function (Deng *et al*, 2009). Telomere fusions in Tpp1-depleted *SNM1B/Apollo* null MEFs is reduced to basal levels only when wild-type Apollo, but not the exonuclease-defective mutant, is reconstituted, further documenting the importance of the SNM1B/Apollo's nuclease activity in mediating this telomere-end protection phenotype in G2.

Factors that generate the 3′ ss overhang at the leading-strand telomere

SNM1B/Apollo is one of several proteins implicated in the protection of leading-strand telomeres after DNA replication. We and others have shown that the MRN complex has a function in protecting leading-strand telomeres after DNA replication (Attwooll *et al*, 2009; Deng *et al*, 2009; Dimitrova and de Lange, 2009). The nuclease activity of Mre11 is involved in the generation of a 3′ ss overhang at the leading-stand, as in the setting of Mre11 nuclease deficiency, leading–leading telomere chromatid-type fusions are generated (Deng *et al*, 2009). However, deletion of Mre11 alone does not result in telomere defects at the leading strand, as this phenotype is only manifested when Trf2 is also removed from telomeres. Likewise, overexpression of the a dominant-negative allele of TRF2 ($TRF2^{\Delta B \Delta M}$) also prevents MRN association with chromosomes, so the chromatid-type

leading-strand telomere fusion phenotype observed is likely due to the combined absence of both TRF2 and MRN from telomeres (Bailey *et al*, 2001; Dimitrova and de Lange, 2009). Elimination and/or depletion of the NHEJ protein DNA-PKcs also results in deprotection of leading-strand telomeres and chromatid-type fusion (Bailey *et al*, 2001; Zhang *et al*, 2005); however, considering the plethora of plausible candidates as physiological substrates for DNA-PKcs kinase activity, which interestingly includes SNM1C/Artemis (the closely related nuclease of SNM1B/Apollo), it is most likely that DNA-PKcs does not act alone at telomeres.

Taken together, these results support SNM1B/Apollo as a major factor involved in protecting leading-strand telomeres after replication from engaging in NHEJ-mediated repair. Importantly, we have recently shown that SNM1B/Apollo physically interacts with Mre11 and Rad50 (Bae *et al*, 2008), suggesting that SNM1B/Apollo might form a complex with the MRN complex at leading-strand telomeres to promote the generation of the 3′ ss overhang.

Materials and methods

Generation of MEFs

MEFs from E13.5 embryos were obtained from the following crosses: *SNM1B/Apollo*$^{+/-} \times$ *SNM1B/Apollo*$^{+/-}$; *SNM1B/Apollo*$^{+/-}$ *Ku70*$^{+/-} \times$ *SNM1B/Apollo*$^{+/-}$*Ku70*$^{+/-}$ and *SNM1B/Apollo*$^{+/-}$ *ATM*$^{+/-} \times$ *SNM1B/Apollo*$^{+/-}$*ATM*$^{+/-}$. E13.5 embryos were isolated, genotyped and immortalized at passage 2 with pBabeSV40LT. Culture conditions were as described earlier (Wu *et al*, 2006).

Vectors and antibodies

Full-length mouse *SNM1B/Apollo* cDNA in frame with 3′ FLAG epitope tag was obtained by PCR amplification from an EST IMAGE clone 5315370 and was cloned into pQCXIP vector (Novex) for retroviral expression. *SNM1B/Apollo* mutation constructs were generated using site-directed mutagenesis according to the manufacturer's instructions (Strategene). All constructs were verified by DNA sequencing. shTRF2 was as described (Deng *et al*, 2009). shTPP1 and TPP1$^{\Delta RD}$ were as described (Guo *et al*, 2007). pLPC-mycTRF2$^{\Delta B \Delta M}$ and anti-mouse TRF1 were kind gifts from Jan Karlseder, Salk Institute. Antibodies used are as follows: γ-tubulin, FLAG and Myc from Sigma; γ-H2AX (no. 05-636) from Upstate and anti-RAP1 from Cell Signaling.

Retroviral infections

Virus-containing supernatant was collected at 36 and 60 h post-transfection and MEFs were infected consecutively two times every 24 h. To obtain cells expressing two different constructs, cells were infected by individual viral supernatants 12 h apart consecutively for two times. For metaphase spread, cells were split 24 h after the last infection and incubated for additional 96 h with a split the day before harvest. During incubation, cells were grown in the culture medium with puromycin at 2.5 μg/ml final concentration. For TIF analysis, cells were processed 24 h after the last infection.

Telomere length and G-strand overhang assays

In-gel G-overhang assays were performed essentially as described (Wu *et al*, 2006). After pulse-field gel electrophoresis (BioRad), gels were dried at 45°C and prehybridized at 50°C for 1 h in Church mix (0.5 M Na_2HPO_4, pH 7.2, 1 mM EDTA and 7% SDS), followed by hybridization at 50°C overnight with γ-^{32}P-$(CCCTAAA)_4$ oligonucleotide. After hybridization, gels were washed three times with 4 × SSC for 30 min and additional three times with 4 × SSC, 0.1% SDS. Gels were exposed to PhosphoImager screens. After G-overhang assays, gels were alkali denatured (0.5 M NaOH and 1.5 M NaCl), neutralized (3 M NaCl and 0.5 M Tris–HCl, pH 7.0), rinsed with H_2O and reprobed with γ-^{32}P-$(CCCTAAA)_4$ oligonucleotide at 55°C and then processed as earlier described. To determine the relative overhang signal, the signal intensity for each lane was determined before and after denaturation using ImageJ. The G-overhang signal was normalized to the total telomeric DNA and this normalized value was compared between samples.

Immunofluorescence and TIF analysis

Immunofluorescence and TIF analysis assays for cells grown on eight-well chamber were performed as described (Guo *et al*, 2007) using the primary antibody TRF1, FLAG and γ-H2AX. Secondary antibodies against mouse or rabbit were labelled with Alexa 488 (Molecular Probes). For the TIF assay, the same primary and secondary antibodies were used with a Tam-OO-$(CCCTAA)_4$ PNA telomere probe (Applied Biosystems). Slides were mounted in vectashield fluorescent mounting media with DAPI (Vector Labs). Digital images were acquired and analysed using a Nikon Eclipse 800 microscope equipped with SBIG STL-11000XM, ST10, ST2000X, ST402ME and Photometrics CCD cameras and processed with Photoshop and CCD Stack software as described earlier (Guo *et al*, 2007). Only cells with at least four γ-H2AX signals co-localized with telomere signals were scored.

Telomere CO-FISH

Cells were grown in the presence of 10 μM BrdU:BrdC (3:1) for 12 h and colcemid was added for the last 5 h at a concentration of 0.2 μg/ml. Cells were harvested by trypsinization, swollen in 0.6 M KCl, fixed in methanol:acetic acid (3:1) and spread on glass slides to obtain the metaphase spreads. CO-FISH was preformed as described earlier (Bailey *et al*, 2001). Metaphase spreads were hybridized sequentially with 5′-Tam-OO-$(CCCTAA)_4$-3′ and 5′-FITC-OO-$(TTAGGG)_4$-3′ probes (Applied Biosystems). A minimum of 2000 chromosomes were scored for each genotype. Images were captured and processed with Metamorph Premiere (Molecular Devices) and processed.

Supplementary data

Supplementary data are available at *The EMBO Journal* Online (http://www.embojournal.org).

Acknowledgements

YCL acknowledges generous support from the MDACC Odyssey Scholars program. SMB gratefully acknowledges support from NASA (NNJ04HD83G and NNX08AB65G). RJL acknowledges support by NCI grant CA052461. SC acknowledges generous financial support from the NIA (RO1 AG028888), the NCI (RO1 CA129037), the Welch Foundation, the Susan G Koman Race for the Cure Foundation, the Abraham and Phyllis Katz Foundation and the Michael Kadoorie Cancer Genetics Research Program. The work in the EG laboratory is supported by the Association pour la Recherche sur le Cancer and the European Union (FP7-Telomarker, Health-F2-2007-200950).

Conflict of interest

The authors declare that they have no conflict of interest.

References

Ahkter S, Richie CT, Zhang N, Behringer RR, Zhu C, Legerski RJ (2005) Snm1-deficient mice exhibit accelerated tumorigenesis and susceptibility to infection. *Mol Cell Biol* **25:** 10071–10078

Akhter S, Legerski RJ (2008) SNM1A acts downstream of ATM to promote the G1 cell cycle checkpoint. *Biochem Biophys Res Commun* **377:** 236–241

Akhter S, Richie CT, Deng JM, Brey E, Zhang X, Patrick Jr C, Behringer RR, Legerski RJ (2004) Deficiency in SNM1 abolishes an early mitotic checkpoint induced by spindle stress. *Mol Cell Biol* **24:** 10448–10455

Attwooll CL, Akpinar M, Petrini JH (2009) The mre11 complex and the response to dysfunctional telomeres. *Mol Cell Biol* **29:** 5540–5551

Bae JB, Mukhopadhyay SS, Liu L, Zhang N, Tan J, Akhter S, Liu X, Shen X, Li L, Legerski RJ (2008) Snm1B/Apollo mediates replication fork collapse and S Phase checkpoint activation in response to DNA interstrand cross-links. *Oncogene* **27:** 5045–5056

Bailey SM, Cornforth MN, Kurimasa A, Chen DJ, Goodwin EH (2001) Strand-specific postreplicative processing of mammalian telomeres. *Science* **293:** 2462–2465

Beucher A, Birraux J, Tchouandong L, Barton O, Shibata A, Conrad S, Goodarzi AA, Krempler A, Jeggo PA, Lobrich M (2009) ATM and Artemis promote homologous recombination of radiation-induced DNA double-strand breaks in G2. *EMBO J* **28:** 3413–3427

Cabuy E, Newton C, Joksic G, Woodbine L, Koller B, Jeggo PA, Slijepcevic P (2005) Accelerated telomere shortening and telomere abnormalities in radiosensitive cell lines. *Radiat Res* **164:** 53–62

Callebaut I, Moshous D, Mornon JP, de Villartay JP (2002) Metallo-beta-lactamase fold within nucleic acids processing enzymes: the beta-CASP family. *Nucleic Acids Res* **30:** 3592–3601

Chen Y, Yang Y, van Overbeek M, Donigian JR, Baciu P, de Lange T, Lei M (2008) A shared docking motif in TRF1 and TRF2 used for differential recruitment of telomeric proteins. *Science* **319:** 1092–1096

d'Adda di Fagagna F, Reaper PM, Clay-Farrace L, Fiegler H, Carr P, Von Zglinicki T, Saretzki G, Carter NP, Jackson SP (2003) A DNA damage checkpoint response in telomere-initiated senescence. *Nature* **426:** 194–198

Dell'Angelica EC, Mullins C, Bonifacino JS (1999) AP-4, a novel protein complex related to clathrin adaptors. *J Biol Chem* **274:** 7278–7285

Demuth I, Bradshaw PS, Lindner A, Anders M, Heinrich S, Kallenbach J, Schmelz K, Digweed M, Meyn MS, Concannon P (2008) Endogenous hSNM1B/Apollo interacts with TRF2 and stimulates ATM in response to ionizing radiation. *DNA Repair (Amst)* **7:** 1192–1201

Demuth I, Digweed M, Concannon P (2004) Human SNM1B is required for normal cellular response to both DNA interstrand crosslink-inducing agents and ionizing radiation. *Oncogene* **23:** 8611–8618

Denchi EL, de Lange T (2007) Protection of telomeres through independent control of ATM and ATR by TRF2 and POT1. *Nature* **448:** 1068–1071

Deng Y, Guo X, Ferguson DO, Chang S (2009) Multiple roles for MRE11 at uncapped telomeres. *Nature* **460:** 914–918

Dimitrova N, de Lange T (2009) Cell cycle-dependent role of MRN at dysfunctional telomeres: ATM signaling-dependent induction of non-homologous end joining (NHEJ) in G1 and resection-mediated inhibition of NHEJ in G2. *Mol Cell Biol* **29:** 5552–5563

Dronkert ML, de Wit J, Boeve M, Vasconcelos ML, van Steeg H, Tan TL, Hoeijmakers JH, Kanaar R (2000) Disruption of mouse SNM1 causes increased sensitivity to the DNA interstrand cross-linking agent mitomycin C. *Mol Cell Biol* **20:** 4553–4561

Ferreira MG, Cooper JP (2001) The fission yeast Taz1 protein protects chromosomes from Ku-dependent end-to-end fusions. *Mol Cell* **7:** 55–63

Ferreira MG, Miller KM, Cooper JP (2004) Indecent exposure: when telomeres become uncapped. *Mol Cell* **13:** 7–18

Freibaum BD, Counter CM (2006) hSnm1B is a novel telomere-associated protein. *J Biol Chem* **281:** 15033–15036

Freibaum BD, Counter CM (2008) The protein hSnm1B is stabilized when bound to the telomere-binding protein TRF2. *J Biol Chem* **283:** 23671–23676

Geng L, Zhang X, Zheng S, Legerski RJ (2007) Artemis links ATM to G2/M checkpoint recovery via regulation of Cdk1-cyclin B. *Mol Cell Biol* **27:** 2625–2635

Guo X, Deng Y, Lin Y, Cosme-Blanco W, Chan S, He H, Yuan G, Brown EJ, Chang S (2007) Dysfunctional telomeres activate an ATM-ATR-dependent DNA damage response to suppress tumorigenesis. *EMBO J* **26:** 4709–4719

Haber JE (2000) Partners and pathwaysrepairing a double-strand break. *Trends Genet* **16:** 259–264

Hartlerode AJ, Scully R (2009) Mechanisms of double-strand break repair in somatic mammalian cells. *Biochem J* **423:** 157–168

Hazrati A, Ramis-Castelltort M, Sarkar S, Barber LJ, Schofield CJ, Hartley JA, McHugh PJ (2008) Human SNM1A suppresses the DNA repair defects of yeast pso2 mutants. *DNA Repair (Amst)* **7:** 230–238

Hockemeyer D, Daniels JP, Takai H, de Lange T (2006) Recent expansion of the telomeric complex in rodents: two distinct POT1 proteins protect mouse telomeres. *Cell* **126:** 63–77

Konishi A, de Lange T (2008) Cell cycle control of telomere protection and NHEJ revealed by a ts mutation in the DNA-binding domain of TRF2. *Genes Dev* **22:** 1221–1230

Lenain C, Bauwens S, Amiard S, Brunori M, Giraud-Panis MJ, Gilson E (2006) The Apollo 5′ exonuclease functions together with TRF2 to protect telomeres from DNA repair. *Curr Biol* **16:** 1303–1310

Li X, Hejna J, Moses RE (2005) The yeast Snm1 protein is a DNA 5′-exonuclease. *DNA Repair (Amst)* **4:** 163–170

Lieber MR, Ma Y, Pannicke U, Schwarz K (2003) Mechanism and regulation of human non-homologous DNA end-joining. *Nat Rev Mol Cell Biol* **4:** 712–720

Liu L, Akhter S, Bae JB, Mukhopadhyay SS, Richie CT, Liu X, Legerski R (2009) SNM1B/Apollo interacts with astrin and is required for the prophase cell cycle checkpoint. *Cell Cycle* **8:** 628–638

Ma Y, Pannicke U, Schwarz K, Lieber MR (2002) Hairpin opening and overhang processing by an Artemis/DNA-dependent protein kinase complex in nonhomologous end joining and V(D)J recombination. *Cell* **108:** 781–794

Miyazaki T, Bressan DA, Shinohara M, Haber JE, Shinohara A (2004) *In vivo* assembly and disassembly of Rad51 and Rad52 complexes during double-strand break repair. *EMBO J* **23:** 939–949

Moshous D, Callebaut I, de Chasseval R, Corneo B, Cavazzana-Calvo M, Le Deist F, Tezcan I, Sanal O, Bertrand Y, Philippe N, Fischer A, de Villartay JP (2001) Artemis, a novel DNA double-strand break repair/V(D)J recombination protein, is mutated in human severe combined immune deficiency. *Cell* **105:** 177–186

Palm W, de Lange T (2008) How shelterin protects mammalian telomeres. *Annu Rev Genet* **42:** 301–334

Pannicke U, Ma Y, Hopfner KP, Niewolik D, Lieber MR, Schwarz K (2004) Functional and biochemical dissection of the structure-specific nuclease ARTEMIS. *EMBO J* **23:** 1987–1997

Poinsignon C, Moshous D, Callebaut I, de Chasseval R, Villey I, de Villartay JP (2004) The metallo-beta-lactamase/beta-CASP domain of Artemis constitutes the catalytic core for V(D)J recombination. *J Exp Med* **199:** 315–321

Richie CT, Peterson C, Lu T, Hittelman WN, Carpenter PB, Legerski RJ (2002) hSnm1 colocalizes and physically associates with 53BP1 before and after DNA damage. *Mol Cell Biol* **22:** 8635–8647

Rooney S, Alt FW, Lombard D, Whitlow S, Eckersdorff M, Fleming J, Fugmann S, Ferguson DO, Schatz DG, Sekiguchi J (2003) Defective DNA repair and increased genomic instability in Artemis-deficient murine cells. *J Exp Med* **197:** 553–565

Smogorzewska A, Karlseder J, Holtgreve-Grez H, Jauch A, de Lange T (2002) DNA ligase IV-dependent NHEJ of deprotected mammalian telomeres in G1 and G2. *Curr Biol* **12:** 1635–1644

Takai H, Smogorzewska A, de Lange T (2003) DNA damage foci at dysfunctional telomeres. *Curr Biol* **13:** 1549–1556

van Overbeek M, de Lange T (2006) Apollo, an Artemis-related nuclease, interacts with TRF2 and protects human telomeres in S phase. *Curr Biol* **16:** 1295–1302

Verdun RE, Crabbe L, Haggblom C, Karlseder J (2005) Functional human telomeres are recognized as DNA damage in G2 of the cell cycle. *Mol Cell* **20:** 551–561

Wang F, Podell ER, Zaug AJ, Yang Y, Baciu P, Cech TR, Lei M (2007) The POT1-TPP1 telomere complex is a telomerase processivity factor. *Nature* **445:** 506–510

Wang H, Zhang X, Geng L, Teng L, Legerski RJ (2009) Artemis regulates cell cycle recovery from the S phase checkpoint by promoting degradation of cyclin E. *J Biol Chem* **284:** 18236–18243

Wu L, Multani AS, He H, Cosme-Blanco W, Deng Y, Deng JM, Bachilo O, Pathak S, Tahara H, Bailey SM, Behringer RR, Chang S (2006) Pot1 deficiency initiates DNA damage checkpoint activation and aberrant homologous recombination at telomeres. *Cell* **126:** 49–62

Xin H, Liu D, Wan M, Safari A, Kim H, Sun W, O'Connor MS, Songyang Z (2007) TPP1 is a homologue of ciliate TEBP-beta and interacts with POT1 to recruit telomerase. *Nature* **445:** 559–562

Ye J, Lenain C, Bauwens S, Rizzo A, Saint-Léger A, Poulet A, Magdinier F, Morere J, Amiard S, Britton S, Calsou P, Salles B, Bizard A, Nadal M, Salvati E, Sabatier L, Wu Y, Biroccio A, Londoño-Vallejo A, Giraud-Panis MJ *et al* (2010) TRF2 and Apollo cooperate with Topoisomerase 2α to protect human telomeres from replicative damage. *Cell* (doi:10.1016/j.cell.2010.05.032)

Zhang Q, Williams ES, Askin KF, Peng Y, Bedford JS, Liber HL, Bailey SM (2005) Suppression of DNA-PK by RNAi has different quantitative effects on telomere dysfunction and mutagenesis in human lymphoblasts treated with gamma rays or HZE particles. *Radiat Res* **164** (4 Part 2)**:** 497–504

Zhang X, Succi J, Feng Z, Prithivirajsingh S, Story MD, Legerski RJ (2004) Artemis is a phosphorylation target of ATM and ATR and is involved in the G2/M DNA damage checkpoint response. *Mol Cell Biol* **24:** 9207–9220

Zhang X, Zhu Y, Geng L, Wang H, Legerski RJ (2009) Artemis is a negative regulator of p53 in response to oxidative stress. *Oncogene* **28:** 2196–2204